
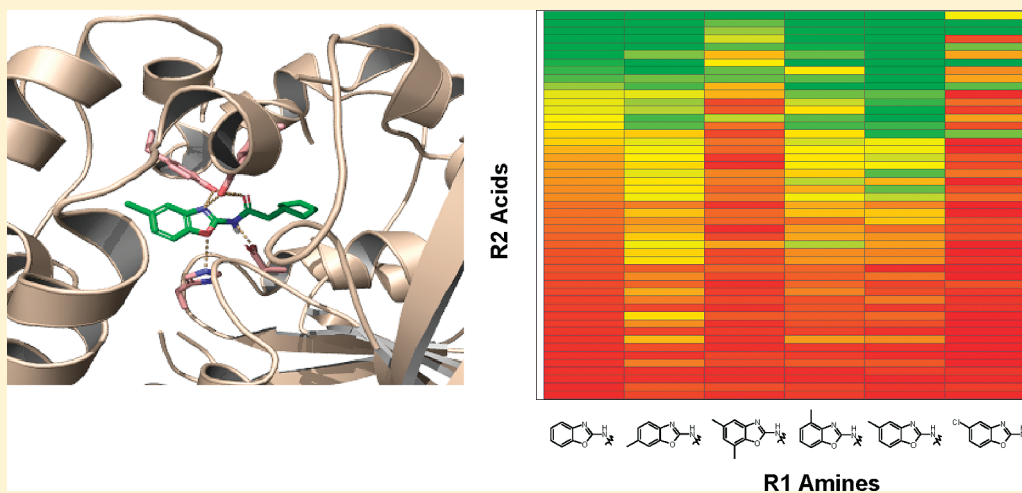


# Discovery of Potent Inhibitors of Soluble Epoxide Hydrolase by Combinatorial Library Design and Structure-Based Virtual Screening<sup>†</sup>

Li Xing,<sup>‡,§,\*</sup> Joseph J. McDonald,<sup>‡</sup> Steve A. Kolodziej,<sup>‡</sup> Ravi G. Kurumbail,<sup>‡</sup> Jennifer M. Williams,<sup>‡</sup> Chad J. Warren,<sup>‡</sup> Janet M. O'Neal,<sup>‡</sup> Jill E. Skepner,<sup>‡</sup> and Steven L. Roberds<sup>‡</sup><sup>‡</sup>Pfizer Global Research and Development, 700 Chesterfield Parkway West, Chesterfield, Missouri 63017, United States<sup>§</sup>Pfizer Global Research and Development, 200 CambridgePark Drive, Cambridge, Massachusetts 02140, United States Supporting Information**ABSTRACT:**

Structure-based virtual screening was applied to design combinatorial libraries to discover novel and potent soluble epoxide hydrolase (sEH) inhibitors. X-ray crystal structures revealed unique interactions for a benzoxazole template in addition to the conserved hydrogen bonds with the catalytic machinery of sEH. By exploitation of the favorable binding elements, two iterations of library design based on amide coupling were employed, guided principally by the docking results of the enumerated virtual products. Biological screening of the libraries demonstrated as high as 90% hit rate, of which over two dozen compounds were single digit nanomolar sEH inhibitors by  $IC_{50}$  determination. In total the library design and synthesis produced more than 300 submicromolar sEH inhibitors. In cellular systems consistent activities were demonstrated with biochemical measurements. The SAR understanding of the benzoxazole template provides valuable insights into discovery of novel sEH inhibitors as therapeutic agents.

**INTRODUCTION**

Oxidative metabolism of arachidonic acid yields a class of potent biological lipids collectively referred to as the eicosanoids.<sup>1</sup> These lipid mediators act physiologically to modulate a variety of cellular activities and play a role in pathophysiology of many illnesses, especially inflammatory and cardiovascular diseases. Two arachidonic acid oxidative enzyme systems, cyclooxygenases and lipoxygenases, are well studied, the inhibition of which have yielded important anti-inflammatory drugs. The third major family of arachidonic acid oxidative enzymes, cytochrome P450s, also generates physiologically important eicosanoids.<sup>2</sup>

Epoxyeicosatrienoic acids (EETs) are cytochrome P450-derived eicosanoids.<sup>3,4</sup> When synthesized in endothelial cells, EETs produce vasodilation and inhibit cytokine-induced inflammatory responses in the vasculature, heart, and kidney.<sup>5–7</sup> The major

catabolic pathway of EETs is catalyzed by soluble epoxide hydrolase (sEH), which converts EETs to biologically less active and more rapidly excreted dihydroxyeicosatrenoic acids (DHETs). In this hydrolyzing function of incorporating the oxirane into the vicinal diol product, sEH shows a high degree of selectivity for lipid epoxides including the regioisomeric EETs. Inhibition of sEH circumvents the major metabolic pathway of EETs, thus enhancing their circulating concentrations and the associated beneficial biological responses. Effective sEH inhibitors have the potential of treating cardiovascular dysfunction and preventing renal damage.<sup>8–12</sup>

Received: September 9, 2010

Published: February 08, 2011

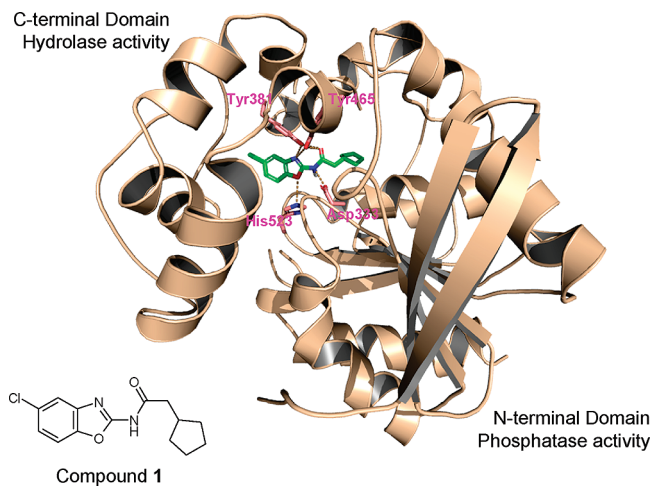
sEH is a member of the  $\alpha/\beta$  hydrolase fold family of enzymes. It forms homodimers with each monomer containing two domains with distinct activities. The N-terminal domain possesses phosphatase activity but is not involved in epoxide hydrolysis.<sup>13,14</sup> The epoxide hydrolase activity resides exclusively in the C-terminal domain, which possesses an  $\alpha/\beta$ -sheet core domain and a lid domain.<sup>15,16</sup> The catalytic unit, situated between the  $\alpha/\beta$  hydrolase fold domain and the lid domain, contains an Asp-His-Asp catalytic triad and two neighboring tyrosine residues in the lid domain, Tyr381 and Tyr465, pointing toward the active site cavity. The catalytic mechanism proceeds via an  $S_N2$ -type reaction in which the epoxide is activated by hydrogen bonds with Tyr381 and/or Tyr465 and undergoes nucleophilic attack by Asp333 to form an alkyl enzyme intermediate, which subsequently collapses into the diol product via incorporation of a water molecule activated by His523.<sup>15,17–20</sup>

A small molecule inhibitor blocking the hydrolase activity of sEH intersects directly the catalytic machinery. The hallmark of such binding interaction consists of simultaneous hydrogen bonds with the two tyrosine residues on the lid and with the catalytic Asp333 from the  $\alpha/\beta$ -sheet domain. Such hydrogen bonds are usually instituted by a urea or amide moiety of the inhibitor molecule. Urea-containing inhibitors,<sup>21–23</sup> arylamides,<sup>24</sup> and piperidylureas<sup>25</sup> have been cocrystallized with mammalian sEH. Elucidated by high-resolution X-ray crystal structures, the residues of the sEH active site are conformationally rigid in general, regardless of whether the catalytic pocket is occupied by a urea inhibitor or not.<sup>22,23,26,27</sup>

Using sEH crystal structures for virtual screening, we designed combinatorial libraries to facilitate the discovery of potent sEH inhibitors based on a benzoxazole template linked to the amide moiety. Surveying commercially available sources, we identified more than 2000 reagents to form the benzoxazole-based products. With the aid of primary binding interactions elucidated by crystal structure, we evaluated plausible binding of the virtual products by computational docking experiments. In place of the docking scores, we applied the distances of the critical inhibitor–enzyme hydrogen bonds as measures of goodness-of-fit. Virtual screening selected over 500 products for synthesis, of which nearly 400 compounds were synthesized. Biological assay of the library and compounds from the follow up libraries yielded exceptionally high hit rates and multiple single-digit nanomolar sEH inhibitors, testifying to the success of virtual screening. The enhanced understanding of the structure–activity relationship (SAR) for the benzoxazole series helps accelerate the design and discovery of novel potent sEH inhibitors.

## RESULTS

**Crystal Structure of Benzoxazole Compound Bound in sEH.** From our screening effort the benzoxazole compound **1** emerged as a potent sEH inhibitor ( $IC_{50} = 32$  nM). To understand its interaction, the crystal structure of **1** bound to the active site of sEH was determined by cocrystallization of the ligand with the C-terminal domain. Depicted in Figure 1, the compound binds deeply within the active site of sEH, forming a network of hydrogen-bonding interactions with key protein atoms. The amide nitrogen of the ligand forms a hydrogen bond with one of the oxygen atoms of the catalytic aspartate residue, Asp333. The carbonyl oxygen of the ligand forms H-bonds with the hydroxyl group of Tyr381 and the side chain amide nitrogen of Glu382. The hydroxyl group of Tyr465 is within hydrogen-bonding distances of the carbonyl oxygen and



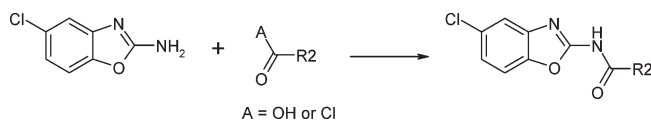
**Figure 1.** Molecular structure of sEH inhibitor compound **1** and its binding interactions illustrated by X-ray crystal structure of its complex in the human sEH hydrolase domain. The benzoxazole nitrogen and the amide oxygen form concurrent hydrogen bonds (dotted lines) with the two tyrosine residues of the lid domain, Tyr381 and Tyr465, respectively. Additional hydrogen bonds are formed between the ligand and His523 and Asp333 of the catalytic triad. The structure is generated using PyMOL.<sup>39</sup>

the nitrogen of the benzoxazole moiety of the inhibitor, although the geometry is imperfect. The oxygen atom of the benzoxazole group is engaged in a strong hydrogen-bonding interaction with the imidazole side chain of His523. The 5-chlorobenzoxazole moiety occupies the smaller of the two lipophilic pockets in the sEH active site, forming van der Waals interactions with several hydrophobic amino acids including Phe265, Phe385, Leu395, Leu406, Met418, Leu427, and Trp524. The larger, solvent exposed pocket of the sEH active site is occupied by the cyclopentyl group of the ligand which forms stacking interaction with the indole side chain of Trp334 and is engaged in van der Waals contacts with the side chains of Met337 and Leu498. The crystal structure also reveals the presence of several well-defined solvent molecules in the larger lipophilic pocket of sEH which could be potentially displaced to further optimize the binding affinity of the compound.

In summary X-ray crystallography revealed a novel interaction mode of the benzoxazole amide template with the sEH hydrolase domain: the hydrogen bonds with the two tyrosine residues are shared by the carbonyl oxygen and the benzoxazole nitrogen of compound **1**, which in turn directs the amide NH straight to the Asp333 side chain.

**Compound Library Design.** Revealed by X-ray crystallography, the enhanced hydrogen bonds with the tyrosine residues via the benzoxazole moiety are novel to known sEH inhibitors. As a result, the benzoxazole template is perceived to achieve high efficiency of sEH inhibition. To efficiently explore the SAR within this chemical space that exploits such favorable binding interactions, a combinatorial library approach was undertaken in pursuit of potent sEH inhibitors. On the basis of our internal experience with dozens of published and internal X-ray crystal structures, molecular docking was predictive of small molecule binding to the sEH protein. In order to fully take advantage of the rich structural information of sEH, docking and virtual screening were employed as the primary engine to the generate binding hypothesis for the virtual library compounds.

Scheme 1



In addition to discovering potent sEH inhibitors, we aimed to improve the ADME properties of **1**, especially its poor metabolic stability (10% remaining in microsomal metabolic stability assay) and low solubility (4  $\mu\text{M}$  kinetic solubility). It has a relatively high ClogP value of 4.2, to which a significant contribution comes from the cyclopentyl moiety. It was conjectured that the unprotected aliphatic groups could undergo rapid metabolism by cytochrome P450 enzymes.<sup>28</sup> Therefore, lowering ClogP was a strategy we apply to alleviate the metabolic burden in the final products of the combinatorial library. Molecular properties that were tailored under the rule of 5 and beyond are MW, ClogP, and tPSA.<sup>29,30</sup>

Molecular modeling suggested that the benzoxazole pocket of sEH binding site is relatively enclosed, limiting the size of functional groups that could possibly fit in. On the acid side of the molecule, on the other hand, the pocket is less constricted; hence, an abundance of chemical variations are allowed. The pocket eventually extends into the solvent without encountering much steric restriction. Therefore, our initial focus was to identify the cyclopentyl replacements of **1** by exploring the relatively open pocket of the sEH binding site to derive both potent sEH inhibition and improved ADME properties. Accordingly the one-dimensional exploration used the 5-chlorobenzoxazole as the single amine of choice.

By use of vendors of commercially reliable sources and removing the reagents that contain diacids or other multifunctions that may interfere with the reaction scheme, a total of 2654 acids and/or acid chlorides were found as possible building blocks for the benzoxazole library. The acids and/or acid chlorides were then combined with the 5-chlorobenzoxazoleamine to form the amide products (Scheme 1). The transformed products were docked into the sEH hydrolase active site as a means to evaluate the goodness of fit for the individual acids and/or acid chlorides.

**Docking and Virtual Screening.** Molecular docking has been proven a valuable tool in screening a large number of compounds in silico and selecting the best candidates for synthesis and biological testing. However, accurately predicting binding free energy of a given protein–ligand complex is yet an ongoing endeavor of computational research.<sup>31,32</sup> Knowing this limitation of the theoretical prediction, we avoided using docking scores as the determining criteria for compound selection but as a guidance to infer reasonable fit of a candidate in the binding site while visual inspection of large number of docking poses became challenging. Rather, given the critical role of Tyr381, Tyr465, and Asp333 of the sEH active site in recognizing the inhibitor binding, we used the strength of the hydrogen bonds formed between these residues and the amide moiety of the inhibitor, measured by their respective heavy atom distances, as the selection criterion of final products.

The hydrogen bond distances with the tyrosine and aspartate residues are highly correlated ( $r^2 = 0.99$ , Figure S1). Such high synergy is consistent with the structural revelation, where the hydrogen bonds engaging both sides of the trans amide moiety anchor the inhibitor into the narrow channel of the sEH binding site. On the other hand, the energy scores showed only moderate correlations with the hydrogen bond distance (Table S2),

possibly a reflection of poor performance of scoring functions in estimating binding affinity as discussed previously. By application of a distance cutoff of 2.8 Å for both hydrogen bonds to the tyrosine and aspartate residues, 574 reagents were selected. They exhibited favorable energies by different scoring methods; i.e., the most favorable values for FlexXscore, DockScore, PMFscore, chemScore, and GoldScore are  $-16.3$ ,  $-71.2$ ,  $-83.8$ ,  $-30.1$ , and  $-104.1$  kcal/mol, respectively. For the next round of selection the hydrogen bond distance criteria were loosened up to 3.5 Å in a search for additional fit by visual inspection of docking generated binding complex. Nineteen additional acids were salvaged for their representation of different chemical space from the ones that were already pooled in. The final selection of 591 reagents, accounting for 22% of the entire collection of suitable carboxylic acids and/or acid chlorides, was submitted for synthesis via combinatorial chemistry.

**sEH Inhibition.** A fluorometric in vitro enzyme assay was used to identify compounds that inhibit soluble epoxide hydrolase activity. The hydrolysis of a surrogate substrate, 6,8-difluoro-4-methylumbelliferyl *trans*-2,3-epoxy-3-phenylpropylcarbonate (DIFMUEC), by purified recombinant sEH was used to measure inhibition of sEH activity. Hydrolysis of the surrogate substrate by sEH causes cyclization and release of umbelliferone, which acts as the assay readout with an excitation at 360 nm and emission at 460 nm. The higher the relative fluorescence unit (RFU), the more product is produced through sEH activity. Each compound was tested in four measurements to yield an average percent inhibition.

Out of the 591 products designed, the first one-dimensional library was delivered in two batches with a total of 383 compounds synthesized, corresponding to a synthetic success rate of 65%. Figure 2a depicts molecular weight and ClogP distributions of this library. The compounds were tested in two batches. The first batch contained 143 compounds that were tested at 10  $\mu\text{M}$  screening concentration in the sEH enzyme assay. The results corroborated an outstandingly high hit rate of 89% at a cutoff of 50% inhibition (Table 1). As a consequence, the screening concentration was lowered to 1  $\mu\text{M}$  to test the second batch of 240 compounds. Similarly, compounds that exhibited 50% inhibition or greater were deemed hits. This stringent criterion yielded a remarkable hit rate of 65%, conveying that about two-thirds of this batch of compounds are nanomolar sEH inhibitors. Figure 3 displays the distribution of percent inhibition for compounds in the one-dimensional library, demonstrating robust enrichment of potent sEH inhibitors delivered by rational design.

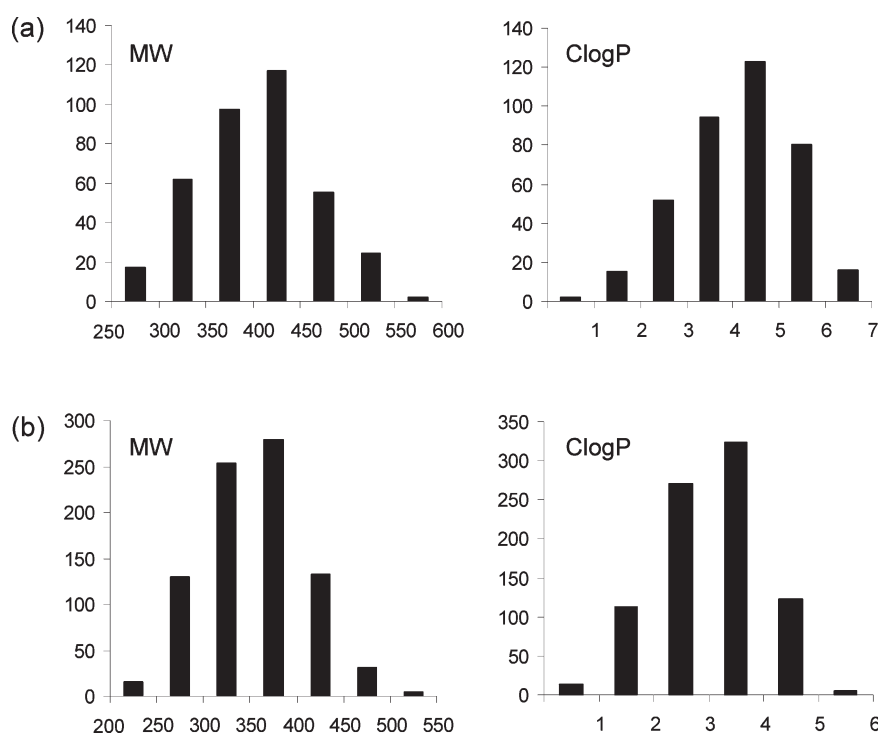
To afford consistent discussion for the second batch of the one-dimensional compounds, their percent inhibition at 10  $\mu\text{M}$  was calculated from the corresponding  $\text{IC}_{50}$ , if one is available (see next section on  $\text{IC}_{50}$ ),

$$\% \text{ inhibition} = \frac{[\text{inhibitor}]}{[\text{inhibitor}] + \text{IC}_{50}}$$

where [inhibitor] denotes the inhibitor concentration. In the absence of  $\text{IC}_{50}$  values, the % inhibition at 10  $\mu\text{M}$  was converted from 1  $\mu\text{M}$  % inhibition using the following equation:

$$\% \text{ inhibition}_2 = \frac{\% \text{ inhibition}_1 [\text{inhibitor}]_2}{\% \text{ inhibition}_1 [\text{inhibitor}]_2 + (1 - \% \text{ inhibition}_1) [\text{inhibitor}]_1}$$

The distribution of percent sEH inhibition after the conversion is plotted in Figure 3b. It is apparent that the converted percent

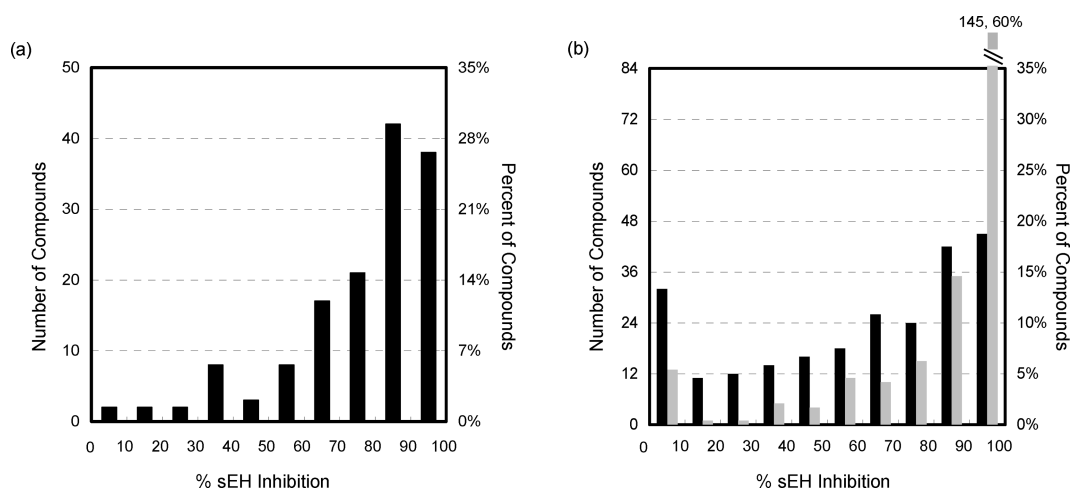


**Figure 2.** Distribution of molecular weight and ClogP properties for the first one-dimensional library (a) and the second two-dimensional library (b). The second iteration library further improves on molecular weight and ClogP (toward lower trend) compared to the first library.

**Table 1. Summary of Synthesis and sEH Activities of Compounds from the One-Dimensional Library<sup>a</sup>**

batch	no. compds proposed	no. compds delivered	screening concn ( $\mu\text{M}$ )	no. sEH active <sup>b</sup>	% sEH active <sup>b</sup>
1	591	143	10	127	88.8%
2		240	1	155 (216)	64.6% (90.0%)

<sup>a</sup> Active compounds are defined as >50% sEH inhibition at the screening concentration. <sup>b</sup> Number in parentheses corresponds to the result after converting to 10  $\mu\text{M}$  screening concentration. Conversion of percent inhibition to 10  $\mu\text{M}$  is described in Results.



**Figure 3.** Distribution of percent inhibitions against sEH enzyme of the one-dimensional library: (a) 143 compounds tested at 10  $\mu\text{M}$ ; (b) 240 compounds tested at 1  $\mu\text{M}$  (black box) and converted to 10  $\mu\text{M}$  (gray box). Each compound is measured for four data points to produce an average percent inhibition.

inhibition has a similar distribution as the first batch (Figure 3a) after they are converted to the same screening concentration. Subsequent discussions will be based on actual or calculated percent inhibition at a consistent 10  $\mu\text{M}$  concentration for all compounds.

In our practice the library design is primarily driven by the theoretically predicted strength of the critical ligand–protein hydrogen bonds. It is curious to investigate how the results may have differed if the selection of final products had been guided by

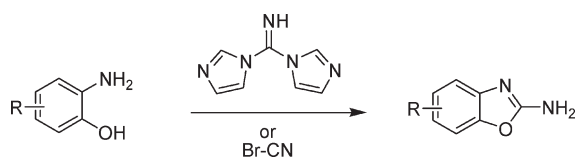
Table 2. Hit Rate Comparison of Hydrogen Bond Distances and Docking Scores

	H-bond distance	FlexXscore	DockScore	PMFscore	ChemScore	GoldScore
no. active compds	343	86	82	101	115	116
hit rate, %	90.0	22.5	21.4	26.4	30.0	30.3

Table 3. Summary of Activity Ranges of the sEH Inhibitors from the One-Dimensional Library

	no. compds	hit rate, %
IC <sub>50</sub> < 10 nM	23	10.3
IC <sub>50</sub> < 100 nM	79	35.4
IC <sub>50</sub> < 1 μM	192	86.1
IC <sub>50</sub> < 10 μM	223	100.0

## Scheme 2



the docking scores. To address that question, we let each scoring function select its top ranking 591 candidate compounds and retrospectively compared the hit rates in Table 2. It is intriguing that all of the scoring functions are far less effective than the interaction-based virtual scoring, yielding at best one-third of the active compounds that were discovered by our undertaken strategy. These results once again speak to the deficiency of scoring functions, as they are designed to be rapidly evaluated and applicable across heterogeneous receptors and ligands.

**IC<sub>50</sub> Determinations.** The active compounds identified by primary enzymatic screening were followed up by IC<sub>50</sub> determinations. A total of 223 compounds were tested for their IC<sub>50</sub> values. The number of compounds at different ranges of sEH activities is summarized in Table 3. All of the compounds were confirmed to have IC<sub>50</sub> values below 10 μM, of which 192 were submicromolar sEH inhibitors. Seventy-nine compounds exhibited less than 100 nM activity, and 23 of them were single-digit nanomolar inhibitors. The ensuing IC<sub>50</sub> values confirmed the hits from the primary screening and substantiated the modeling predictions.

**Follow-Up Two-Dimensional Library.** On the basis of analysis of the crystal structures, we predicted that there would be room for small substitutions off the benzoxazole ring. To expand the learning from the one-dimensional library and to develop structure–activity relationship of benzoxazole variations, a follow-up library was designed. Two-dimensional combinations of different amines and acids were instituted in a parallel matrix. The benzoxazole templates were derived from a number of aminophenols via nucleophilic ring formation using di(imidazole-1-yl)-methanimine as the one-carbon source (Scheme 2).<sup>33</sup>

Eight aminophenols were selected to form a small diverse set of substituted benzoxazoles. The substituted benzoxazoles were then coupled with a smaller number of acids to form the final products using Scheme 1. Approximately 200 acids were selected from the one-dimensional library for amide coupling based on three considerations. First, compounds containing chiral centers that are not critical are removed to reduce molecular complexity. Since the sEH binding pocket is bottlenecked around the amide moiety, we

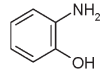
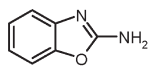
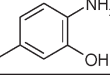
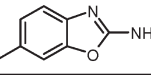
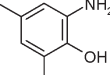
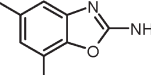
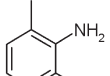
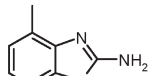
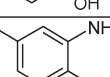
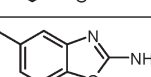
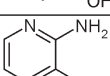
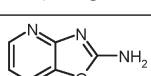
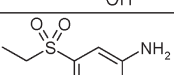
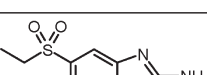
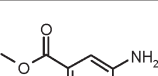
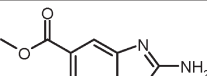
visually inspected the acids that contain a stereogenic carbon α to the forming amide bond. It was therefore decided to keep the cyclic stereocenters and remove the acyclic ones that are less attractive. Second, more stringent ClogP criteria were applied, bringing most of the final products into the range of ClogP < 3. Third, we chose a structurally diverse subset of acids, attempting to cover more or less the same chemical space as the one-dimensional library. As a result, 218 acids were selected to react with the eight aminophenol derived benzoxazoles to form the final products.

Figure 2b shows a histogram of the molecular weight and ClogP for the second iteration library. Compared to compounds in the first library, both molecular weight and ClogP are trended toward the lower values, indicating continued optimization of these properties. Results of the two-dimensional library are summarized in Table 4. The unsubstituted benzoxazoles showed respectable sEH activity. Methyl substituted benzoxazoles displayed differentiated preference for sEH interaction. In decreasing hit rates they are ordered by 5,7-dimethyl-, 4-methyl-, 6-methyl-, and 5-methylbenzoxazoles. Modeling predicted that large and polar functional groups are detrimental for the benzoxazole pocket because of the limited size and the hydrophobic nature of the pocket. In keeping with the prediction, low hit rates were displayed by 5-ethylsulfonyl and 5-methyl ester benzoxazoles. The intolerance of polarity of the benzoxazole pocket is further asserted by the oxazolopyridine entry, in which case a single carbon to nitrogen atom change abolished sEH activity of 96 compounds.

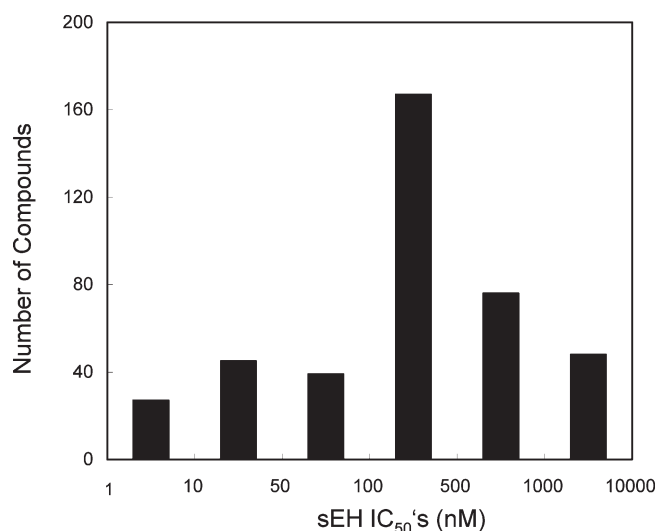
**SAR of Benzoxazole Series.** By application of docking-based virtual screening to the combinatorial library design, a number of potent sEH inhibitors were discovered. Depicted in Figure 4 is the distribution of compounds in different ranges of IC<sub>50</sub> values. Of all the compounds tested out of the one-dimensional and two-dimensional libraries, 291 compounds (88%) are nanomolar sEH inhibitors. The remaining compounds range from 1 to 10 μM in activity. Extremely potent sEH inhibitors were identified, of which 27 compounds showed single digit nanomolar IC<sub>50</sub> values.

Examples of potent sEH inhibitors are given in Table 5, with their IC<sub>50</sub> values ranging from 3 to 270 nM. We hypothesized at our design stage that lowering ClogP would result in sEH inhibitors with improved metabolic stability and solubility. In Table 5 none of the exemplified compounds have ClogP values exceeding 4.5, with most of the ClogP values below 3. Stability of the compounds in the presence of human liver microsomes was assessed and is represented in Table 5 as percentage of the remaining parent compound after 30 min of incubation. It is notable that we have improved the metabolic stability of this set of compounds upon the initial lead compound **1** (10% remaining). Compounds **1a**, **1g**, and **1i** all demonstrated greater than 50% remaining in the microsomal assay. The compounds were further characterized using an in vitro COS-7 cell-based assay to identify inhibitors of sEH which are cell-permeable and active on native enzyme with endogenous substrate. Consistent translation from the sEH enzyme assay to the cellular activities was observed. In general the cellular data correlate well with the biochemical measurement. Compounds **1b**, **1c**, **1d**, **1h**, **1i**, and **1j** are identified as single digit nanomolar sEH inhibitors in the cell.

Table 4. Summary of Synthesis and sEH Activities of the Two-Dimensional Library<sup>a</sup>

entry	nucleophile	benzoxazole reagent	no. comps produced	no. sEH active	% sEH active
1			89	57	64.0
2			99	50	50.5
3			104	77	74.0
4			72	44	61.1
5			139	57	41.0
6			96	0	0.0
7			107	25	23.4
8			134	12	8.96

<sup>a</sup> Active compounds are defined as >50% sEH inhibition at 10  $\mu$ M.

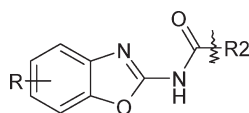


**Figure 4.** Distribution of compounds by sEH IC<sub>50</sub> values, ranging between 1 nM and 10  $\mu$ M. A total of 402 compounds out of the library design have passed >50% inhibition from the primary screening and are determined for their IC<sub>50</sub> values. Each IC<sub>50</sub> curve is an 11-point titration in duplicate.

Two-dimensional heat map provides an overall SAR picture. In Figure 5, compounds of different couplings of R1 amines and R2 acids are presented by sEH enzyme inhibition. The leading

column, the unsubstituted benzoxazole as R1, serves as the baseline. From analysis of crystal structures it is appreciated that the 5-chlorobenzoxazole occupies a hydrophobic pocket of sEH, being in close contact with the side chains of Phe265, Leu427, Leu406, and Pro266. Therefore, removal of 5-chloro is anticipated to reduce potency, and this is confirmed by comparing compounds in entry 1 of the two-dimensional library with those from the one-dimensional library. Noted in Figure 5 for pairwise comparisons of the benzoxazole and 5-chlorobenzoxazole compounds, the 5-chloro substituent principally renders the compounds more potent than the unsubstituted benzoxazole analogs.

Entry 5 of the two-dimensional library installs a methyl replacement of chloro on the benzoxazole, a bioisosteric transformation frequently applied in medicinal chemistry. Comparing direct analogues of 5-methylbenzoxazole and 5-chlorobenzoxazole indicates that such replacement engendered noticeable differences in sEH inhibition. The 5-chloro analogues are in general more active than the 5-methyl compounds. This is perceived to be a ClogP effect. As illustrated in Table 5, the ClogP increases by 5-chloro and 5-methyl additions to benzoxazole are 0.8 and 0.5 units, respectively. Therefore, by incursion of a slightly higher lipophilicity, the 5-chlorobenzoxazole compounds could outperform their 5-methylbenzoxazole direct analogues by more favorable desolvation as well as stronger hydrophobic interaction in the benzoxazole pocket of sEH. Consistent and yet marginal trends are displayed by IC<sub>50</sub> comparisons in Figure 6.

Table 5. Examples of sEH Inhibitors Discovered by Library Design<sup>a</sup>

comps	R	R2	ClogP	sEH IC <sub>50</sub> (nM)	COS-7 cell IC <sub>50</sub> (nM)	human liver microsomal stability (% remaining)
1a	H		3.43	94.3	10.3	83
1b	5-Cl		4.23	6.92	1.54	43
1c	5-Me		3.93	11.4	0.486	6
1d	5,7-diMe		4.42	73	4.38	22
1e	4-Me		3.93	272	NT	NT
1f	6-Me		3.93	202	NT	NT
1g	H		2.67	19.4	22.0	62
1h	5-Cl		3.47	3.58	4.68	45
1i	5-Me		3.17	3.61	5.76	53
1j	5,7-diMe		3.67	46.5	1.42	22
1k	4-Me		3.17	109	NT	NT
1l	6-Me		3.17	184	NT	NT

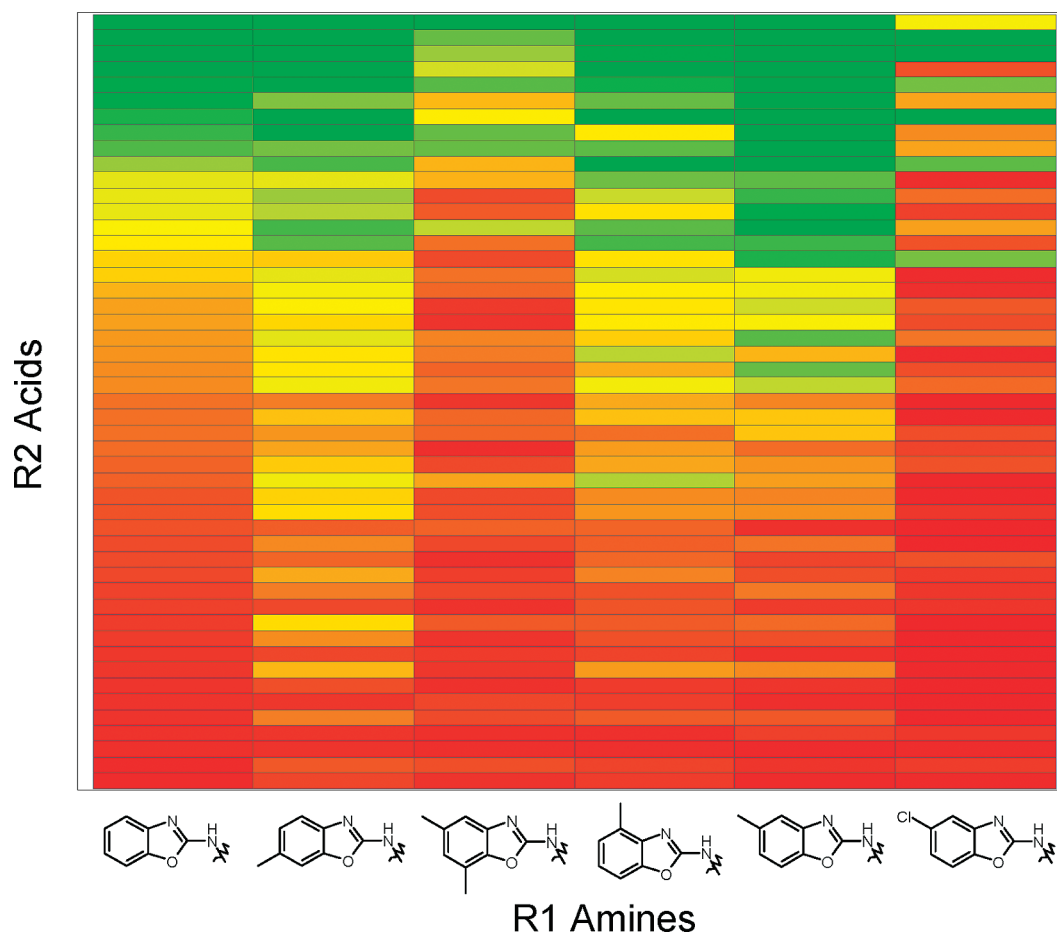
<sup>a</sup> NT: not tested.

In IC<sub>50</sub> comparisons in Figure 6 it is apparent that either 4- or 6-methyl substitution off the benzoxazole generally cause loss of activity by a magnitude of approximately 10-fold compared to the unsubstituted benzoxazoles. On the other hand, small substituents off 5-benzoxazole are beneficial to activity by filling up the hydrophobic subpocket, demonstrated by improvement in activity of both 5-methyl- and 5-chlorobenzoxazoles over the unsubstituted benzoxazoles. Methyl and chloro appear to be

good bioisosteres of each other, yielding analogues of comparable sEH potencies.

## DISCUSSION

It is observed that 6-methyl substitution is detrimental to sEH inhibition in general, while 5-methylbenzoxazole improves potency compared to unsubstituted benzoxazole. Modeling suggested that the 6-methyl off the benzoxazole shall poke into the



**Figure 5.** Heat map of sEH compounds, colored by percent inhibition at 10  $\mu\text{M}$  in gradients: 100% is red, 50% is yellow, and 0% is green. The  $x$ -axis represents six benzoxazole amines, and the  $y$ -axis depicts different acid reagents.

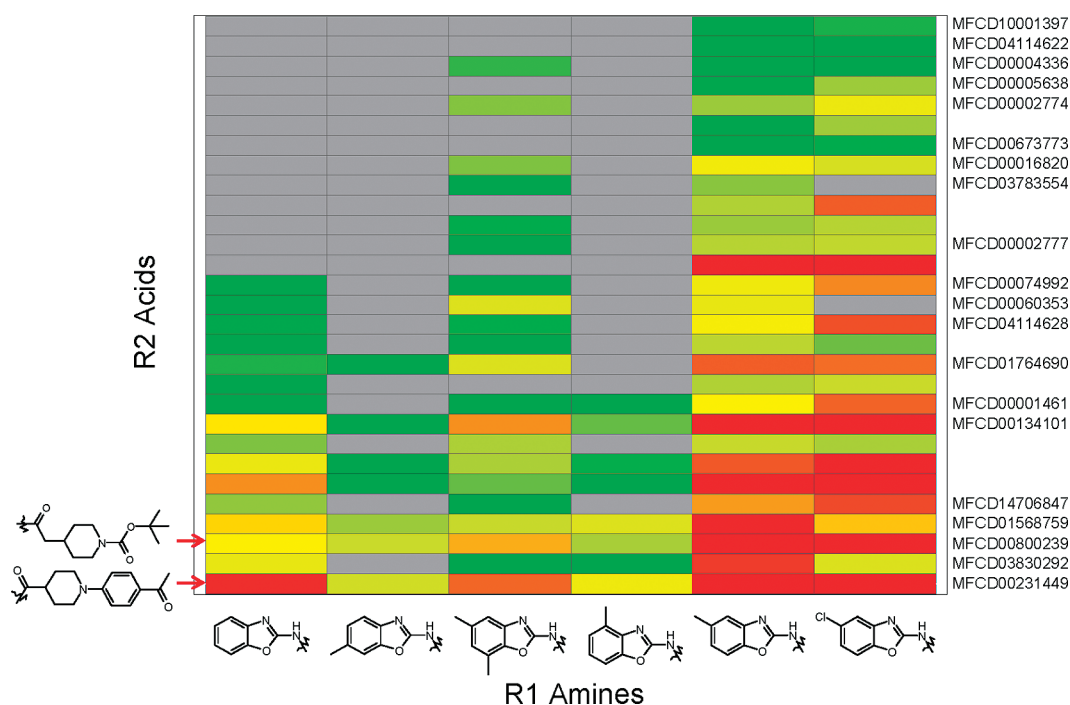
sEH pocket if the benzoxazole ring remains in the orientation elucidated by the crystal structure. In order to avoid steric clashes with the protein, the 6-methylbenzoxazole likely undergoes a  $180^\circ$  rotation along the connecting bond between the benzoxazole and the amide to direct the 6-methyl into the same hydrophobic subpocket as the 5-methyl off the benzoxazole. In the flipped conformation the critical hydrogen bonds with the tyrosine residues are preserved by the benzoxazole oxygen atom in place of the nitrogen. Despite their seemingly comparable abilities for accepting protons, the hydrogen bond to the oxygen atom is much weaker than to the nitrogen in the benzoxazole system. Theoretical calculations showed that the hydrogen bond to oxazole nitrogen is more stable than to oxygen by as high as 10 kJ/mol in energy.<sup>34</sup> Survey of crystal structures of organic molecules confirmed that the frequency of hydrogen bonds to nitrogens largely outnumbers that to oxygens when they are both available in a competing situation of heterocycles.<sup>34,35</sup> This difference in hydrogen bond strength rejects symmetry of benzoxazole and presumably accounts for the activity loss of the 6-methylbenzoxazole from the 5-methylbenzoxazole compounds.

The 5,7-dimethylbenzoxazoles displayed respectable sEH activities when combined with a number of acids. On the basis of modeling, the benzoxazole undergoes a slight rotation around the connecting bond to amide from the crystal structure to direct the 7-methyl to the open channel of the binding pocket. The 4-methylbenzoxazoles, on the other hand, displayed significant

loss of activities. This could be rationalized by modeling analysis, which suggested that in the standing conformation represented by compound **1** the 4-methyl is crashing into the side chains of His523 and Trp524. One possible way to alleviate the steric clash is that the benzoxazole ring flips along the 2-benzoxazole bond so that the 4-methyl points to the open channel, in a spatial location that is equivalent to the 7-methyl discussed in the 5,7-dimethylbenzoxazoles. In such orientation the benzoxazole oxygen would accept the protons from Tyr381 and Tyr465, which based on previous discussion, is a much weaker interaction than the hydrogen bond with the benzoxazole nitrogen. Therefore the 4-methylbenzoxazoles are less active against sEH for similar reasons to the 6-methylbenzoxazoles.

Although predicted binding modes may be considered generally reliable, current scoring functions are found to have very limited accuracy in ranking compounds from diverse series or indeed even from homologous series. Over the past two decades significant amounts of effort have been put into refining the scoring functions to accurately predict the binding free energies, at least in the relative sense, so they can be used for rank ordering if not for quantitative measures of activities. Nevertheless, given the complexity of the ligand–protein binding process and the approximations made in calculating desolvation and entropic terms, the docking scores have not proven accurate in predicting binding affinities.<sup>36–38</sup> Progress can be made through the derivation of a broader range of descriptors relevant to receptor–ligand binding.





**Figure 6.** Heat map of sEH compounds, colored by  $IC_{50}$  values in gradient: 10 nM and less (red), 100 nM (yellow), and 1000 nM and greater (green). The *x*-axis represents six benzoxazole amines, and the *y*-axis depicts different acid reagents.

On the other hand, it is more productive, based on our experience, that docking scores are treated as general guidance of goodness-of-fit and combined with more accurate measures of the tightness-of-fit by specific molecular parameters that reflect the essence of the binding event. Such parameters could be derived from monitoring the critical hydrogen bonds discussed in this study, the geometry of an essential  $\pi$ - $\pi$  stacking, and/or the occupation of a hydrophobic pocket that prepositions the ligand in the binding site. In order to apply different computational strategies to virtual screening in an effective manner, it is paramount that the unique interactions that drive ligand binding to the specific biological target are thoroughly understood.

## CONCLUSION

Structure-based virtual screening was successfully applied to the design of combinatorial libraries based on a benzoxazole template exemplified by lead compound **1** to discover novel and potent sEH inhibitors. Critical ligand-protein hydrogen bond formation of the modeled binary complexes was utilized as the major selection criteria. The first library focused on the coupling of 591 acids with the 5-chlorobenzoxazoleamine. Of the 383 final compounds synthetically delivered 90% are tested active in the sEH enzyme assay, corroborating the high success rate of the design. Subsequent  $IC_{50}$  determination confirmed 23 compounds as single digit nanomolar sEH inhibitors. Retrospective analysis of docking scores computed by five different scoring functions suggested that they were less effective at differentiating good binders from poor ones than the hydrogen bond criteria used in the design. The second combinatorial library further explored the SAR by the amide bond formation between a subset of the acids and eight (aza)benzoxazole amines. Of the 840 compounds produced 322 were active against sEH. Cellular activities demonstrated consistent translation from the sEH enzyme assay results. These studies revealed intriguing SAR of

the benzoxazole template for potent sEH inhibition and valuable insights into discovery of potent and efficacious modulators of this potential therapeutic target.

## EXPERIMENTAL SECTION

**Molecular Modeling.** Transformation of acids and/or acid chlorides according to Scheme 1 to their prototypical products was conducted within Pipeline Pilot 7.5 (Accelrys Software Inc., www.accelrys.com). The products were subsequently standardized by assigning the appropriate protonation states at physiological pH 7.4.

The FlexX program was used for docking calculations. The X-ray structure of the binary complex of sEH and compound **1** was used as the protein model. Docking protocol was tailored to increase the goodness of match to crystal structures. The residues within 6.5 Å of the cocrystal ligand were included in the binding site definition. In order to account for potential charge interactions with several acidic and basic residues within the sEH binding site, “assign formal charges” option was turned on. No partial charges were precomputed but were assigned by the GASTEIGER method during CScore calculation, which included FlexX, DOCK, GOLD, ChemScore, and PMF. In order to account for stereochemistry, the  $sp^3$  nitrogen and the *R/S* carbon centers were allowed to be modified during FlexX runs. The rest of the FlexX parameters were set to default.

For validation compound **1** was extracted out of the crystal complex and redocked into the binding site of sEH. The root mean squared distance (rmsd) between the docked conformation and the crystal structure is 0.95 Å, with the amide and the 5-chlorobenzoxazole moieties closely matching the crystal conformations. Most of the discrepancies arise from the cyclopentyl group, which goes toward the opening of the pocket. Hence, its higher flexibility could be expected.

An SPL (Sybyl programming language) script was written to extract the hydrogen bond distances. For Tyr381/Tyr465 interaction, the shorter distance between the amide carbonyl oxygen and either one of the side chain oxygens of Tyr381 or Tyr465 was registered. For the hydrogen bonds with Asp333 side chain, the distances between the amide

nitrogen of the inhibitor and the two oxygen atoms of the aspartate side chain were measured, and the shorter length was registered.

**X-ray Crystallography.** The C-terminal hydrolase domain of human sEH (amino acids corresponding to 225–555) with an N-terminal thrombin-cleavable hexahistidine tag was expressed in insect cells using a baculovirus expression system. Following cell lysis and centrifugation, the supernatant was purified by Ni affinity chromatography using a HisTrap FF column. The bound sEH protein was eluted with 200 mM imidazole after washing with 30 mM imidazole. Subsequently, the protein was further purified over a Sephacryl S200 column by size exclusion chromatography. The pooled fractions were analyzed by SDS–PAGE and mass spectrometry for purity and evaluated in biochemical assays.

Cocrystals of the His-tagged hydrolase domain reagent complexed with the ligand (1:5 stoichiometry) were generated by hanging drop vapor diffusion experiments at room temperature. Typically, 1  $\mu$ L of protein solution (5–7 mg/mL, 50 mM NaCl, 10% glycerol, 2 mM DTT, 50 mM sodium phosphate at pH 7.4) was mixed with 1  $\mu$ L of precipitant solution (26–30% PEG 6000, 70 mM ammonium acetate, 200 mM magnesium acetate, 100 mM sodium cacodylate at pH 6.5). Crystals appeared overnight and were harvested straight from the drop for diffraction experiments.

Diffraction data were collected to 2.6 Å resolution. The crystal belongs to the space group  $P2_12_12_1$  with unit cell dimensions  $a = 46.523$  Å,  $b = 79.902$  Å, and  $c = 89.318$  Å. The crystal structures of the complex were solved by difference Fourier methods using the known structure of sEH. Electron density maps were calculated after a few cycles of rigid body, positional, and  $B$ -factor refinement. Inhibitors were modeled into the electron density using the program O and further refined using the program X-plor. The structure of the sEH complex was refined to  $R_{\text{work}}$  of 27.9% and  $R_{\text{free}}$  of 33.3%. Complete data collection and refinement statistics are provided in Table S1 of Supporting Information (SI).

#### Compounds and Analytical and Purification Processes.

Compounds were received in 96-well-plate format dissolved in 100% DMSO. The targeted synthetic amount was 100  $\mu$ mol. Then 20  $\mu$ L from each well was transferred to a daughter plate and diluted with 200  $\mu$ L of DMSO. The libraries were analyzed on LC/MS and purified using a 50 mm  $\times$  20 mm C18 column with gradient conditions. The fractions were collected on a Gilson 215 liquid handler at a maximum of 10 mL/tube using pretared tubes. The purified fractions were selected based on comparisons of the purification chromatogram with the prepurification LC/MS analysis, and tubes were combined that contained pure compound. The final selections were analyzed on the LC/MS. Following the analysis, the fractions were evaporated to dryness in Zymark evaporators using nitrogen gas in a water bath at 40 °C. When the tubes were completely dried, they were placed in a 40 °C vacuum oven for 4 h and weighed on a Bohden robot. The final weight was subtracted from the pretared weight to give the quantity of compound present. The tubes containing compounds that passed identity and purity specifications were dissolved in DMSO and transferred to shipment plates. Compounds were purified by chromatography to a purity of at least 95% as determined by HPLC. Purity of the 12 exemplified compounds in Table 5 is provided in Supporting Information Table S3 by HPLC–UV, HPLC–ELSD, and APCI–TIC. Mass spectra were obtained using atmospheric pressure chemical ionization (APCI). Full spectroscopic characterization of all example compounds is provided in the Supporting Information.

**sEH Enzyme Assay.** The chimeric mouse–human sEH enzyme was expressed using a baculovirus system and comprising an N-terminal 6-His domain followed by a thrombin cleavage site and the N-terminal domain of mouse sEH (amino acids 1–222) connected to the C-terminal domain of human sEH (amino acids 224–555). Sequences correspond to GenPept accession numbers NP\_001970 for human sEH and

NP\_031966 for mouse sEH. Insect cells expressing sEH were lysed and centrifuged at 30000g for 30 min at 4 °C. Supernatants were filtered (0.45  $\mu$ m filter) and loaded onto a 5 mL HisTrap FF column (GE Healthcare). After washing in HisTrap buffer and 30 mM imidazole, 6-His-containing protein was eluted with 200 mM imidazole in HisTrap buffer. Fractions containing protein were loaded onto and washed through a HiPrep 16/60 Sephacryl S200 column (GE Healthcare) for preparative size-exclusion chromatography. Before pooling, fractions containing >90% purified full-length protein were identified by SDS–PAGE and analytical size-exclusion chromatography using a BioSil250 column (Bio-Rad Laboratories). Identity of the protein was confirmed by mass spectrometry.

The soluble epoxide hydrolase (sEH) fluorometric assay is an in vitro enzyme assay used to identify compounds that inhibit soluble epoxide hydrolase activity. Instead of the native EET's substrate, the hydrolysis of a surrogate substrate, 6,8-difluoro-4-methylumbelliferyl *trans*-2,3-epoxy-3-phenylpropylcarbonate (DIFMUEC), by sEH was used to follow activity. DIFMUEC (MW = 388.32) was purchased from Invitrogen Molecular Probes (www.invitrogen.com, 100  $\mu$ g/vial) at 99% purity. Characterization results of DIFMUEC are provided in Supporting Information. Conversion of the surrogate substrate by sEH causes cyclization and release of umbelliferone. The assay was performed in 384-well black polystyrene flat bottom plates (Corning no. 3654) in PBS at pH 7.4 (GIBCO no. 10010-023). Compounds dissolved in 1% dimethylsulfoxide (DMSO) were incubated with the sEH enzyme at 1 nM for 10 min at room temperature. The reaction was initiated with the addition of DIFMUEC at 5  $\mu$ M. The reaction was measured kinetically or run as an end point assay with the addition of acetonitrile to 25% final concentration as a stop reagent after 5 min of reaction. Umbelliferone was measured as the assay product with an excitation at 360 nm and emission at 460 nm using a TECAN Safire2 (Tecan Group, San Jose, CA). Relative fluorescence units (RFU) are proportional to the amount of product produced through sEH activity.

Compounds received preliminary biochemical evaluation by determining percent inhibition at 1 and/or 10  $\mu$ M. Those demonstrating 50% or greater inhibition were then tested in an 11-point concentration-response assay in duplicates for  $IC_{50}$  determinations. The inhibition data were fit to a competitive inhibition model to determine  $IC_{50}$  values.

**sEH Cell-Based Assay in COS-7 Cells.** COS-7 cells were spiked with exogenous 11,12-epoxyeicosatrienoic acid (11,12-EET) substrate, and its hydrolysis to 11,12-dihydroxyeicosatrienoic acid (11,12-DHET) was monitored. COS-7 cells (American Type Culture Collection, Manassas, VA) were maintained in high glucose Dulbecco's modified Eagle's medium (Invitrogen, Carlsbad, CA) supplemented with 10% fetal bovine serum (Hyclone, Logan, UT) and 1% penicillin–streptomycin/L-glutamine (Invitrogen) at 37 °C in a humidified atmosphere containing 5% CO<sub>2</sub>. Cells were plated at 30 000 per well in 96-well format and allowed to attach overnight. Inhibitors solubilized in DMSO were added to the wells in a final concentration of 1% DMSO. Cells were incubated with the inhibitors for 1 h at 37 °C. The substrate, 11,12-EET (Cayman Chemical, Ann Arbor, MI), was added to a final concentration of 800 nM, and cells were incubated for an additional 2 h at 37 °C. The cell culture medium was removed and analyzed for 11,12-DHET via LC/MS/MS. Quantification was accomplished by online C-18 trapping of 11,12-DHET (Microm BioResources and Keystone Scientific) followed by liquid chromatography and tandem mass spectrometry. An API-3000 mass spectrometer (Applied Biosystems) was operated in the negative ion turbospray multiple reaction-monitoring mode using Analyst 1.4.1 software. The amount of 11,12-DHET in the sample was determined by normalization of the integrated 11,12-DHET to an octadeuterated 11,12-DHET standard chromatographic signal.

**Microsomal Stability.** Human microsomal assays are performed using pooled microsomes from Gentest to determine the clearance of a

compound due to phase I (including cytochrome P450) metabolism. In humans, variability in P450 expression is a significant factor, so a large number of liver microsome preparations are pooled to represent an average array of P450s. Substrates of 1  $\mu\text{M}$  are added to the 100 mM phosphate buffer (pH 7.4) containing the regenerating system (1 mM NADP<sup>+</sup>, 5 mM isocitric acid, 1 U/mL isocitric dehydrogenase) and cofactor of 1 mM MgCl<sub>2</sub>. The samples are analyzed at the 30 min time point for the remainder of the parent compound.

## ■ ASSOCIATED CONTENT

**S Supporting Information.** Correlation of hydrogen bond distances and energy scores, data collection and refinement statistics for X-ray crystallography, purity and spectroscopic characterization data of new compounds, and purity and characterization of DIFMUEC. This material is available free of charge via the Internet at <http://pubs.acs.org>.

## Accession Codes

<sup>†</sup>The atomic coordinates and structure factors of compound **1** in complex with sEH have been deposited in the Protein Data Bank, [www.rcsb.org](http://www.rcsb.org) (PDB code 3PDC).

## ■ AUTHOR INFORMATION

### Corresponding Author

\*Phone: (617) 665-5369. Fax: (617) 665-5575. E-mail: [li.xing@pfizer.com](mailto:li.xing@pfizer.com).

## ■ ACKNOWLEDGMENT

We thank Bryan Witherbee for important contributions to the design of the enzymatic assay and Harold Woodward for purifying sEH protein for crystallography and activity assays. We also thank the reviewers for their insightful suggestions. This study was sponsored by Pfizer Inc.

## ■ ABBREVIATIONS USED

sEH, soluble epoxide hydrolase; EET, epoxyeicosatrienoic acid; DHET, dihydroxyeicosatrienoic acid; DIFMUEC, 6,8-difluoro-4-methylumbelliferyl *trans*-2,3-epoxy-3-phenylpropylcarbonate; SAR, structure–activity relationship

## ■ REFERENCES

- (1) Funk, C. D. Prostaglandins and leukotrienes: advances in eicosanoid biology. *Science* **2001**, *294*, 1871–1875.
- (2) Node, K.; Huo, Y.; Ruan, X.; Yang, B.; Spiecker, M.; Ley, K.; Zeldin, D. C.; Liao, J. K. Anti-inflammatory properties of cytochrome P450 epoxygenase-derived eicosanoids. *Science* **1999**, *285*, 1276–1279.
- (3) Zeldin Darryl, C. Epoxygenase pathways of arachidonic acid metabolism. *J. Biol. Chem.* **2001**, *276*, 36059–36062.
- (4) Kroetz Deanna, L.; Zeldin Darryl, C. Cytochrome P450 pathways of arachidonic acid metabolism. *Curr. Opin. Lipidol.* **2002**, *13*, 273–283.
- (5) Inceoglu, B.; Schmelzer, K. R.; Morisseau, C.; Jinks, S. L.; Hammock, B. D. Soluble epoxide hydrolase inhibition reveals novel biological functions of epoxyeicosatrienoic acids (EETs). *Prostaglandins Other Lipid Mediators* **2007**, *82*, 42–49.
- (6) Fleming, I. Vascular cytochrome p450 enzymes: physiology and pathophysiology. *Trends Cardiovasc. Med.* **2008**, *18*, 20–25.
- (7) Spector, A. A.; Fang, X.; Snyder, G. D.; Weintraub, N. L. Epoxyeicosatrienoic acids (EETs): metabolism and biochemical function. *Prog. Lipid Res.* **2004**, *43*, 55–90.
- (8) Schmelzer, K. R.; Kubala, L.; Newman, J. W.; Kim, I.-H.; Eiserich, J. P.; Hammock, B. D. Soluble epoxide hydrolase is a therapeutic target for acute inflammation. *Proc. Natl. Acad. Sci. U.S.A.* **2005**, *102*, 9772–9777.

(9) Imig, J. D. Cardiovascular therapeutic aspects of soluble epoxide hydrolase inhibitors. *Cardiovasc. Drug Rev.* **2006**, *24*, 169–188.

(10) Chiamvimonvat, N.; Ho, C.-M.; Tsai, H.-J.; Hammock, B. D. The soluble epoxide hydrolase as a pharmaceutical target for hypertension. *J. Cardiovasc. Pharmacol.* **2007**, *50*, 225–237.

(11) Fang, X. Soluble epoxide hydrolase: a novel target for the treatment of hypertension. *Recent Pat. Cardiovasc. Drug Discovery* **2006**, *1*, 67–72.

(12) Imig, J. D.; Zhao, X.; Zaharis, C. Z.; Olearczyk, J. J.; Pollock, D. M.; Newman, J. W.; Kim, I.-H.; Watanabe, T.; Hammock, B. D. An orally active epoxide hydrolase inhibitor lowers blood pressure and provides renal protection in salt-sensitive hypertension. *Hypertension* **2005**, *46*, 975–981.

(13) Tran, K. L.; Aronov, P. A.; Tanaka, H.; Newman, J. W.; Hammock, B. D.; Morisseau, C. Lipid sulfates and sulfonates are allosteric competitive inhibitors of the N-terminal phosphatase activity of the mammalian soluble epoxide hydrolase. *Biochemistry* **2005**, *44*, 12179–12187.

(14) Cronin, A.; Homburg, S.; Durk, H.; Richter, I.; Adamska, M.; Frere, F.; Arand, M. Insights into the catalytic mechanism of human sEH phosphatase by site-directed mutagenesis and LC-MS/MS analysis. *J. Mol. Biol.* **2008**, *383*, 627–640.

(15) Arand, M.; Wagner, H.; Oesch, F. Asp333, Asp495, and His523 form the catalytic triad of rat soluble epoxide hydrolase. *J. Biol. Chem.* **1996**, *271*, 4223–4229.

(16) Arand, M.; Cronin, A.; Adamska, M.; Oesch, F. Epoxide hydrolases: structure, function, mechanism, and assay. *Methods Enzymol.* **2005**, *400*, 569–588.

(17) Yamada, T.; Morisseau, C.; Maxwell, J. E.; Argiriadi, M. A.; Christianson, D. W.; Hammock, B. D. Biochemical evidence for the involvement of tyrosin in epoxide activation during the catalytic cycle of epoxide hydrolase. *J. Biol. Chem.* **2000**, *275*, 23082–23088.

(18) Langhlin, L. T.; Tzeng, H.-F.; Lin, S.; Armstrong, R. N. Mechanism of microsomal epoxide hydrolase. Semifunctional site-specific mutants affecting the alkylation half-reaction. *Biochemistry* **1998**, *37*, 2897–2904.

(19) Pinot, F.; Grant, D. F.; Beetham, J. K.; Parker, A. G.; Borhan, B.; Landt, S.; Jones, A. D.; Hammock, B. D. Molecular and biochemical evidence for the involvement of the Asp-333-His-523 pair in the catalytic mechanism of soluble epoxide hydrolase. *J. Biol. Chem.* **1995**, *270*, 7968–7974.

(20) Borhan, B.; Jones, A. D.; Pinot, F.; Grant, D. F.; Kurth, M. J.; Hammock, B. D. Mechanism of soluble epoxide hydrolase. Formation of an  $\alpha$ -hydroxy ester-enzyme intermediate through Asp-333. *J. Biol. Chem.* **1995**, *270*, 26923–26930.

(21) Gomez, G. A.; Morisseau, C.; Hammock, B. D.; Christianson, D. W. Structure of human epoxide hydrolase reveals mechanistic inferences on bifunctional catalysis in epoxide and phosphate ester hydrolysis. *Biochemistry* **2004**, *43*, 4716–4723.

(22) Argiriadi, M. A.; Morisseau, C.; Goodrow, M. H.; Dowdy, D. L.; Hammock, B. D.; Christianson, D. W. Binding of alkylurea inhibitors to epoxide hydrolase implicates active site tyrosines in substrate activation. *J. Biol. Chem.* **2000**, *275*, 15265–15270.

(23) Argiriadi, M. A.; Morisseau, C.; Hammock, B. D.; Christianson, D. W. Detoxification of environmental mutagens and carcinogens: structure, mechanism, and evolution of liver epoxide hydrolase. *Proc. Natl. Acad. Sci. U.S.A.* **1999**, *96*, 10637–10642.

(24) Eldrup, A. B.; Soleymanzadeh, F.; Taylor, S. J.; Muegge, I.; Farrow, N. A.; Joseph, D.; McKellop, K.; Man, C. C.; Kukulka, A.; De Lombaert, S. Structure-based optimization of arylamides as inhibitors of soluble epoxide hydrolase. *J. Med. Chem.* **2009**, *52*, 5880–5895.

(25) Eldrup, A. B.; Soleymanzadeh, F.; Farrow, N. A.; Kukulka, A.; De Lombaert, S. Optimization of piperidyl-ureas as inhibitors of soluble epoxide hydrolase. *Bioorg. Med. Chem. Lett.* **2010**, *20*, 571–575.

(26) Gomez, G. A.; Morisseau, C.; Hammock, B. D.; Christianson, D. W. Human soluble epoxide hydrolase: structural basis of inhibition by 4-(3-cyclohexylureido)-carboxylic acids. *Protein Sci.* **2006**, *15*, 58–64.

(27) Gomez, G. A.; Morisseau, C.; Hammock, B. D.; Christianson, D. W. Structure of human epoxide hydrolase reveals mechanistic

inferences on bifunctional catalysis in epoxide and phosphate ester hydrolysis. *Biochemistry* **2004**, *43*, 4716–4723.

(28) Gillam, E. M. Extending the capabilities of nature's most versatile catalysts: directed evolution of mammalian xenobiotic-metabolizing P450s. *Arch. Biochem. Biophys.* **2007**, *464*, 176–186.

(29) Linpinski, C. A.; Lombardo, F.; Dominy, B. W.; Feeney, P. J. Experimental and computational approaches to estimate solubility and permeability in drug discovery and development settings. *Adv. Drug Delivery Rev.* **1997**, *23*, 3–25.

(30) Ertl, P.; Rohda, B.; Selzer, P. Fast calculation of molecular polar surface area as a sum of fragment based contributions and its application to the prediction of drug transport properties. *J. Med. Chem.* **2000**, *43*, 3714–3717.

(31) Waszkowycz, B. Towards improving compound selection in structure-based virtual screening. *Drug Discovery Today* **2008**, *13*, 219–226.

(32) Kolb, P.; Irwin, J. J. Docking screens: right for the right reasons? *Curr. Top. Med. Chem.* **2009**, *9*, 755–770.

(33) Wu, Y.-Q.; Limburg, D. C.; Wilkinson, D. E.; Hamilton, G. S. Formation of nitrogen-containing heterocycles using di(imidazole-1-yl)-methanimine. *J. Heterocycl. Chem.* **2003**, *40*, 191–193.

(34) Nobeli, I.; Price, S. L.; Lommerse, J. P. M.; Taylor, R. Hydrogen bonding properties of oxygen and nitrogen acceptors in aromatic heterocycles. *J. Comput. Chem.* **1997**, *18*, 2060–2074.

(35) Bohm, H. J.; Brode, S.; Hesse, U.; Klebe, G. Oxygen and nitrogen in competitive situations: Which is the hydrogen-bond acceptor? *Chem.—Eur. J.* **1996**, *2*, 1509–1513.

(36) Leach, A. R.; Shoichet, B. K.; Peishoff, C. E. Prediction of protein–ligand interactions. Docking and scoring: successes and gaps. *J. Med. Chem.* **2006**, *49*, 5851–5855.

(37) O'Boyle, N. M.; Liebeschuetz, J. W.; Cole, J. C. Testing assumptions and hypotheses for rescoring success in protein–ligand docking. *J. Chem. Inf. Model.* **2009**, *49*, 1871–1878.

(38) Kitchen, D. B.; Decornez, H.; Furr, J. R.; Bajorath, J. Docking and scoring in virtual screening for drug discovery: methods and applications. *Nat. Rev. Drug Discovery* **2004**, *3*, 935–949.

(39) *The PyMOL Molecular Graphics System*, version 1.3; Schrodinger, LLC.: New York; <http://www.pymol.org>.